sustainability

MDPI

Article

Carbon-Stock Estimation Using High-Resolution Remote Sensing Imagery at Universitas Padjadjaran: A Spatial–Temporal Analysis to Support Sustainable and Green Campus Initiatives

Rahmihafiza Hanafi [1], Bakhrul Midad [2], Rania Alifa Desenaldo [3], Bambang Wijatmoko [2], Gemilang Lara Utama Saripudin [4], Muhammad Aufaristama [5], Kusnahadi Susanto [1,2] and Irwan Ary Dharmawan [2,*]

1 Center for Sustainable Campus Development and Environmental Safety, Universitas Padjadjaran, Jl. Ir. Soekarno Km 21, Sumedang 45363, West Java, Indonesia; rahmihafiza.hanafi@unpad.ac.id (R.H.); k.susanto@unpad.ac.id (K.S.)
2 Department of Geophysics, Faculty of Mathematics and Natural Sciences, Universitas Padjadjaran, Jl. Ir. Soekarno Km 21, Sumedang 45363, West Java, Indonesia; bakhrul22001@mail.unpad.ac.id (B.M.); bwmoko@geophys.unpad.ac.id (B.W.)
3 Department of Civil Engineering, Geo and Environmental Sciences, Karlsruhe Institute of Technology, 76131 Karlsruhe, Germany; urkmd@student.kit.edu
4 Department of Food Industrial Technology, Faculty of Agro-industrial Technology, Universitas Padjadjaran, Jl. Ir. Soekarno Km 21, Sumedang 45363, West Java, Indonesia; g.l.utama@unpad.ac.id
5 College of Science, Geosciences Department, United Arab Emirates University, Al Ain 15551, United Arab Emirates; aufaristama@uaeu.ac.ae
* Correspondence: iad@geophys.unpad.ac.id

Abstract

Estimating carbon stocks in semi-urban ecosystems remains challenging due to spatial heterogeneity and the scale limitations of conventional datasets. This study aims to estimate and analyse the spatial and temporal distribution of carbon stocks at Universitas Padjadjaran using high-resolution remote sensing imagery and to support sustainable campus and green campus initiatives. Multi-temporal data from WorldView-2 (2015, 2017), WorldView-3 (2021), and Legion-03 (2025) were used to derive vegetation indices, followed by aboveground biomass (AGB) modelling through regression analysis. Carbon stock was calculated using a standard conversion factor of 0.5. The results show a consistent increase in vegetation density and carbon stock, with average values rising from 20.381 tonnes/ha in 2015 to 29.160 tonnes/ha in 2025. The use of the MSAVI produced an accurate model for predicting AGB (R^2 = 0.987–0.993). This study introduces a novel integration of high-resolution imagery using MSAVI to improve AGB estimation at the campus scale, providing a more detailed and reliable approach for carbon assessment in heterogeneous semi-urban environments and contributing to the implementation of sustainable, environmentally friendly campus management strategies.

Keywords: above ground biomass; carbon stock; high-resolution satellite imagery; vegetation indices; sustainable campus

Academic Editor: Ali Bahadori-Jahromi

Received: 16 April 2026
Revised: 2 June 2026
Accepted: 15 June 2026
Published: 17 June 2026

1. Introduction

Climate change is still considered one of the most serious environmental problems today, mainly because of the increasing concentration of greenhouse gases that affect atmospheric processes and ecosystem functions. Terrestrial ecosystems help reduce these impacts by acting as carbon sinks, storing carbon in vegetation biomass [1,2]. Consequently,

understanding how much carbon vegetation stores is important for understanding the global carbon cycle and the role of ecosystems in climate regulation. Monitoring is also needed to assess how ecosystems change over time and to evaluate the effectiveness of land-based mitigation efforts [3–5]. In addition, at a local scale, such information is increasingly important for supporting sustainability initiatives, including the implementation of green campus programmes that aim to reduce carbon footprints and enhance environmental management in university settings.

Aboveground biomass (AGB) is all living biomass above the soil, including stem, stump, branches, bark, seeds and foliage (IPCC Good Practice Guidance for LULUCF). AGB is often used as an indicator of carbon stock in vegetation because a large portion of the carbon absorbed through photosynthesis is stored in aboveground parts such as stems, branches, and leaves [1]. Therefore, accurately estimating AGB is important for understanding how carbon is distributed and how the balance between carbon sources and sinks operates across different areas. On university campuses, accurate AGB estimation can also provide a scientific basis for planning and evaluating green infrastructure and sustainability strategies [6].

In general, AGB can be estimated using field measurements or remote sensing approaches [7]. Field-based methods usually involve measuring tree diameter, height, and sometimes wood density, which are then used in allometric equations [5]. These methods can give quite accurate results, especially at small scales. However, they are not always practical when the study area is large or highly heterogeneous, mainly because they require significant time, effort, and cost. Increasing the number of samples to achieve a better spatial representation can also be quite challenging logistically. In contrast, remote sensing offers a more practical means of estimating AGB over larger areas. It allows data to be collected consistently and repeatedly without direct field measurements in every location. Different types of remote sensing data, such as optical imagery, SAR, and LiDAR, have been widely used for biomass estimation. For example, LiDAR systems like GEDI can capture the vertical structure of forests, which is very useful for improving biomass estimation accuracy [8].

Among these approaches, optical vegetation indices are still commonly used because they can represent vegetation greenness and photosynthetic activity [9,10]. NDVI is one of the most widely used indices and is often applied as a proxy for leaf area and vegetation productivity [11]. However, these indices also have some limitations. NDVI, for instance, tends to saturate in areas with dense vegetation, making it less sensitive in high-biomass conditions. In addition, optical data are quite sensitive to clouds, atmospheric effects, and lighting conditions, which can affect the results [12]. Therefore, estimating biomass in complex vegetation structures remains challenging. Huete [13] proposed the soil-adjusted vegetation index (SAVI) to reduce soil-reflectance interference in sparsely vegetated areas; Qi et al. [14] subsequently refined it into the modified soil-adjusted vegetation index (MSAVI), which incorporates a self-adjusting correction factor and maintains sensitivity to canopy structure under variable understory conditions. The enhanced vegetation index (EVI) of Huete et al. [15] introduces an atmospheric-resistance term and retains sensitivity in dense canopies where NDVI saturates. The leaf area index (LAI), derived from these indices through empirical or physical formulations [16], is widely used as an intermediate variable linking reflectance to biomass. Ratio-based indices, including the red-green ratio (RGR) and the ratio vegetation index (RVI), have also been applied to characterise vegetation in structurally complex landscapes [17].

In an early review of optical AGB methods, Lu [18] identified vegetation-index regression as the most accessible operational approach while noting saturation in dense canopies as its principal limitation, which has since been mitigated through narrow-band

and soil-adjusted indices [19]. Forkuor et al. [20] combined Sentinel-1 and Sentinel-2 indices to map AGB in West African dryland forests, and Muhe and Argaw [21] developed empirical AGB models for Afro-Montane tropical forests on the basis of LAI alone. Another issue is related to scale. Many global biomass datasets provide broad coverage, but their spatial resolution is often too coarse for smaller or more detailed study areas; by contrast, studies that use high-resolution data are usually limited to specific locations [5]. In smaller, more complex areas, such as university campuses, aboveground biomass (AGB) is commonly estimated using field-based measurements or a combination of field data and remote sensing. These approaches often rely on vegetation indices, such as NDVI, to develop carbon-stock models [22–24]. This situation creates a critical gap, particularly on university campuses, which are relatively small yet characterised by highly heterogeneous vegetation. Consequently, such environments require more detailed and site-specific assessment approaches to effectively support sustainable campus planning and the development of green campus frameworks.

Based on this, the use of high-resolution satellite imagery with vegetation indices still needs further exploration, particularly in semi-urban environments such as campus areas. Therefore, this study aims to estimate carbon stocks on a university campus, specifically at Universitas Padjadjaran (Unpad), by integrating high-resolution satellite data with vegetation indices. This approach is expected to provide AGB estimates and a better understanding of carbon-stock patterns in semi-urban ecosystems without recourse to species-specific field inventories, while also supporting the implementation of sustainable campus and green campus initiatives through improved carbon monitoring and environmental management [8,12].

2. Materials and Methods

2.1. Study Area

This study was carried out at the Unpad Jatinangor Campus in Jatinangor District, Sumedang Regency, West Java, Indonesia (Figure 1). The campus is situated at around 107°46′28″ E and 6°55′33″ S, at elevations of between 725 and 810 metres above sea level. Covering approximately 180 hectares and home to 18 faculties, it ranks among the largest university campuses in Indonesia in terms of land area.

The campus exhibits heterogeneous land cover, characterised by a blend of academic infrastructure and preserved green spaces. The western zone is predominantly an Arboretum, while the northern area includes the Ciparanje experimental field, which serves as a site for agricultural and ecological research. Academic facilities and supporting infrastructure are mainly concentrated in the central and southern regions, creating a complex spatial mosaic of built-up surfaces interspersed with vegetated areas. This structural diversity and spatial heterogeneity position the Unpad Jatinangor Campus as a representative model of an urban campus forest system, making it a suitable study site for examining spatial and temporal variations in carbon stock using high-resolution remote sensing data.

This heterogeneity extends to the species composition of the vegetation itself. Within the Western Arboretum, Aswada et al. [25] documented five named zones, such as rare species, identity tree, industrial medicinal, and fruit-tree, each built around a different mix of tropical hardwoods, native species and horticultural taxa. The most common species recorded across these zones include *Tectona grandis*, *Swietenia macrophylla*, *Hura crepitans*, *Pterocarpus indicus*, *Cedrela odorata*, *Enterolobium cyclocarpum*, *Durio* sp., *Annona muricata* and *Averrhoa carambola*. The wider campus carries a canopy of native hardwoods, fast-growing legumes, ornamental shade trees, and fruit tree species planted under institutional greening programmes since 2016 [26].

Figure 1. Study area: the Unpad Campus (107°46′28″ E, 6°55′33″ S; ~180 ha; elevation 725–810 m.a.s.l.) in West Java, Indonesia, showing the Arboretum (west), Ciparanje experimental field (north), academic building (centre–south), and embung retention pond (centre).

2.2. Data

This study utilised high-resolution satellite imagery acquired from WorldView-2 for the years 2015 and 2017, WorldView-3 for 2020, and WorldView Legion 3 for 2025. Specifications regarding the acquisition dates and spatial resolution of each sensor are provided in Table 1. All datasets were sourced from Maxar Technologies and were chosen for their sub-metre spatial resolution, which allows for the detection of fine-scale variations in urban vegetation despite the comparatively small extent of the study area. The imagery was provided as Ortho Ready Standard (Level 2A) products, which have undergone radiometric correction and been georeferenced to the WGS 84 coordinate system.

Table 1. Summary of satellite data used in this study.

Satellite	Acquisition Date	Panchromatic (m)	Multispectral Resolution (m)
WorldView-2	15 June 2015	0.46	1.84
WorldView-2	20 July 2017	0.46	1.84
WorldView-3	10 July 2020	0.31	1.24
WorldView Legion3	18 May 2025	0.30	1.20

To support vegetation-indices calculation, visible bands (blue, green, and red), Red Edge, and near-infrared (NIR) bands were employed. The full spectral configuration of the WorldView sensors is presented in Table 2 [27].

Table 2. Spectral characteristics of the WorldView satellites [27].

Band	Spectral Range (μm)
Coastal	0.400–0.450
Blue	0.450–0.510
Green	0.510–0.580
Yellow	0.585–0.625
Red	0.630–0.690
Red Edge	0.705–0.745
NIR-1	0.770–0.895
NIR-2	0.860–1.040

2.3. Methodology

The overall methodological workflow is presented in Figure 2. Data processing was conducted using Google Earth Engine and QGIS. Google Earth Engine, a cloud-based platform widely used for processing large-scale satellite imagery and land suitability mapping [28], was employed in this study..Initially, the acquired imagery underwent pre-processing, including atmospheric correction, delineation of the area of interest (AOI) and image preparation. The preprocessing steps comprised defining land cover classes, applying pan-sharpening to enhance spatial resolution, and performing geometric correction to improve positional accuracy [27]. Subsequently, vegetation indices were computed. The initial aboveground biomass (AGB_0) was estimated using the leaf area index (LAI). Each derived index was then subjected to linear regression analysis to generate an improved AGB estimation model. Carbon stock was calculated by multiplying the estimated AGB values by a carbon conversion factor. The developed AGB model was further cross-sensor validated using imagery from the Landsat 8. Linear regression analysis was performed to evaluate the relationship between AGB estimates derived from WorldView Legion 3, WorldView-3, and WorldView-2 (independent variables, x) and those obtained from Landsat 8 (dependent variable, y), with model performance assessed using the coefficient of determination (R^2).

2.4. Preprocessing

To enhance the accuracy and reliability of subsequent analyses, the raw satellite imagery underwent a series of preprocessing steps. All WorldView-2, WorldView-3, and WorldView Legion 3 images underwent atmospheric correction using the Dark Object Subtraction (DOS) method [29] to reduce the influence of atmospheric scattering and absorption on surface reflectance. In this approach, the atmospheric haze for each band is estimated from dark targets within the scene, such as deep water or shadows, which are assumed to have negligible reflectance, and the corresponding path radiance is then subtracted before the top-of-atmosphere values are converted to surface reflectance. DOS was preferred because it is computationally simple and requires no in situ atmospheric data at the time of acquisition, yet has proven reliable for high-resolution imagery in vegetation and carbon-stock studies [30–32].

Pan-sharpening was applied by integrating high-resolution panchromatic bands with lower-resolution multispectral bands to improve spatial detail without compromising spectral information [33]. Before image fusion, the multispectral bands were resampled to match the panchromatic band's spatial resolution using cubic spline interpolation, ensuring precise pixel alignment and minimising spectral distortion. The Brovey transform was

subsequently employed to fuse the spatial detail of the panchromatic data with the spectral characteristics of the multispectral bands, producing a high-resolution dataset suitable for campus-scale analysis. This approach was selected due to its ability to preserve spectral relationships while enhancing spatial detail, making it particularly effective for urban vegetation mapping.

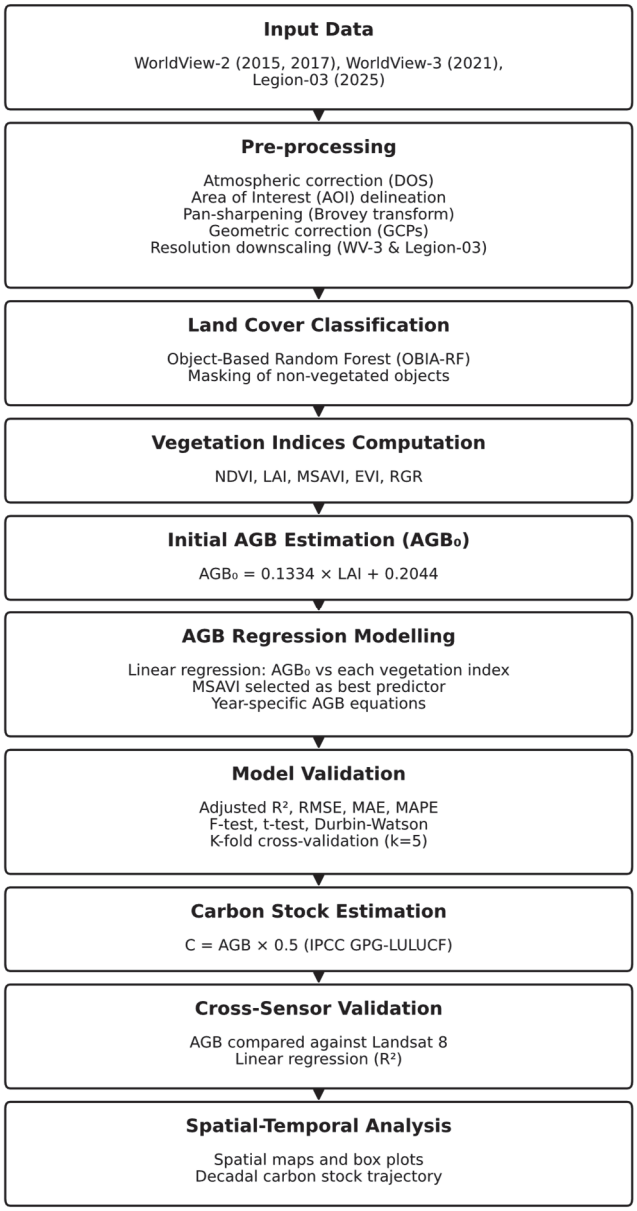

Figure 2. Methodology research flow.

Following this, geometric correction was performed to align image pixels with their correct geographic coordinates and to ensure spatial consistency across multi-temporal datasets. This step is essential for enabling accurate comparison of land cover changes over time [34]. The geometric correction was performed in QGIS to ensure that all imagery was properly aligned and spatially consistent within the study area. In this study, the correction was carried out using Ground Control Points (GCPs) extracted from permanent features such as road intersections and the corners of stable buildings; the number and spatial distribution of GCPs are well established as primary factors controlling the geometric accuracy of corrected very-high-resolution (VHR) satellite imagery, in conjunction with the chosen transformation model [35,36]. A polynomial transformation was then

applied in combination with a cubic B-spline resampling kernel, which yields a smooth interpolated reflectance surface and is recognised for its good frequency response and reduced interpolation error compared with simpler kernels [37].

The WorldView-3 and WorldView Legion 3 imagery were down-sampled to a 50 cm spatial resolution using cubic B-spline interpolation to match the resolution of the WorldView-2 imagery, ensuring spatial consistency across all datasets prior to further analysis. With this procedure, all images were integrated into the projection system adopted for the study and were therefore ready for vegetation-indices analysis.

2.5. Land Cover Masking

To restrict the AGB modelling and carbon-stock estimation to vegetated surfaces, each annual image was further classified into vegetated and non-vegetated categories using the object-based random forest framework previously developed for the same campus [27]. The classification was performed by first partitioning the imagery into spectrally homogeneous objects through segmentation and subsequently assigning each object to one of six land cover classes, namely dense vegetation, sparse vegetation, buildings, roads, bare soil, and water, on the basis of its combined spectral and geometric properties within a random forest classifier trained on manually labelled reference samples. The dense and sparse vegetation classes were then combined into a single vegetation mask, which was applied during the AGB and carbon-stock estimation to ensure that only vegetated pixels contributed to the final outputs. Non-vegetated surfaces, comprising buildings, roads, bare soil, and water, were therefore excluded from the analysis.

2.6. Data Processing and Analysis

The vegetation indices computed in this study are summarised in Table 3. A total of five vegetation indices were analysed. The normalised difference vegetation index (NDVI) is widely used to represent vegetation density and distribution, with values ranging from −1 to 1. Higher NDVI values indicate dense, healthy vegetation, whereas lower values indicate sparse vegetation [38,39]. The enhanced vegetation index (EVI) provides improved sensitivity to canopy structure by reducing atmospheric noise and minimising soil background effects [40]. The modified soil-adjusted vegetation index (MSAVI) is a variant [14]. The leaf area index (LAI) is the ratio of total leaf area to the ground surface area it occupies and is an important biophysical parameter of vegetation [41,42]. The red-green ratio (RGR) is utilised to estimate the extent and quality of vegetation cover within the study area [16].

Table 3. Vegetation indices and chlorophyll indices are applied for the estimation of AGB.

Indices	Equation	Source	Eq
Normalised Difference Vegetation Index (NDVI)	$\mathrm{NDVI} = \frac{(\mathrm{NIR} - \mathrm{RED})}{(\mathrm{NIR} + \mathrm{RED})}$	[15]	(1)
Enhanced Vegetation Index (EVI)	$\mathrm{EVI} = \frac{2.5 \times (\mathrm{NIR} - \mathrm{RED})}{(\mathrm{NIR} + 6 \times \mathrm{RED} - 7.5 \times \mathrm{BLUE} + 1)}$	[43]	(2)
Leaf Area Index	$\mathrm{LAI} = (3.618 \times \mathrm{EVI} - 0.118)$	[16]	(3)
Red Green Index (RGR)	$\mathrm{RGR} = \frac{\mathrm{RED}}{\mathrm{GREEN}}$	[16]	(4)
Modified Soil Adjust Vegetation Index (MSAVI)	$\mathrm{MSAVI} = \frac{0.5 \times \left(2 \times \mathrm{NIR} + 1 - \sqrt{(2 \times \mathrm{NIR} + 1)^2 - 8(\mathrm{NIR} - \mathrm{RED})}\right)}{2 - \mathrm{RED}}$	[14]	(5)

2.7. Above-Ground Biomass (AGB) Modelling Using Remote Sensing

Regression modelling was employed to estimate AGB using the derived vegetation indices. The initial AGB (AGB_0) was calculated using a simple linear regression model based on the LAI, expressed as: AGB_0 = 0.1334 LAI + 0.2044 [16]. This equation provides a species-agnostic biomass proxy calibrated in tropical canopies and has recently been validated by Thinley et al. [16] in a subtropical urban Arboretum with multi-species composition comparable to the Unpad campus area.

Following the estimation of AGB_0, further regression analyses were conducted to examine the relationships between AGB and the remaining vegetation indices. The LAI and EVI were excluded from this stage because they had already been incorporated into the initial modelling framework. Simple linear regression models were applied to develop improved AGB estimation models. Model accuracy was evaluated using the coefficient of determination (R^2) and its adjusted form, the root-mean-square error (RMSE), mean absolute error (MAE) and mean absolute percentage error (MAPE). The significance of each regression and of its coefficients was tested with the F- and t-statistics at $\alpha = 0.001$, and residual autocorrelation was assessed with the Durbin–Watson statistic. Model generalisability was confirmed by five-fold cross-validation.

$$\mathrm{RMSE} = \sqrt{\frac{1}{n}\sum_{i=1}^{n}(y_i - \widehat{y}_i)^2} \tag{6}$$

$$\mathrm{MAE} = \frac{1}{n}\sum_{i=1}^{n}|y_i - \widehat{y}_i| \tag{7}$$

$$\mathrm{MAPE} = \frac{100\%}{n}\sum_{i=1}^{n}\left|\frac{y_i - \widehat{y}_i}{y_i}\right| \tag{8}$$

2.8. Carbon-Stock Estimation

The selected AGB model was subsequently applied to estimate carbon stock across the study area. AGB was converted to carbon using a factor of 0.5, the IPCC GPG-LULUCF default for the carbon fraction of aboveground biomass, defined as all living biomass above the soil, including stem, stump, branches, bark, seeds, and foliage [44]. The same factor has been widely used in urban green-space carbon studies on heterogeneous canopies, including Nowak and Crane [45] for urban trees in the United States, Sun et al. [46] for Beijing and Wu et al. [47] for Lishui. As the Unpad campus is dominated by living biomass above soil, such as trees, seeds and foliage, the 0.5 factor is appropriate and ensures comparability with these studies.

3. Results

3.1. Temporal and Spatial Variation in Vegetation Indices

The temporal analysis demonstrated a consistent increase in median values across all vegetation indices from 2015 to 2025 (Figure 3), indicating a progressive improvement in vegetation cover and condition. NDVI increased from 0.711 to 0.819, with its interquartile range contracting substantially (from 0.206 to 0.042) by 2025. Although this indicates denser and more spatially uniform vegetation, the marked compression of the distribution also suggests NDVI saturation in the later years, as the index becomes less sensitive under closed-canopy conditions. EVI, by contrast, retained a broader distribution and a steady increase (0.284 to 0.502), demonstrating greater sensitivity in densely vegetated areas. MSAVI followed a similar increasing trend (0.234 to 0.431) while maintaining a stable spread, consistent with its reduced susceptibility to soil background effects. LAI showed

the most substantial change, with its median nearly doubling (0.911 to 1.698), in agreement with the increasing leaf density and structural complexity of the canopy over time.

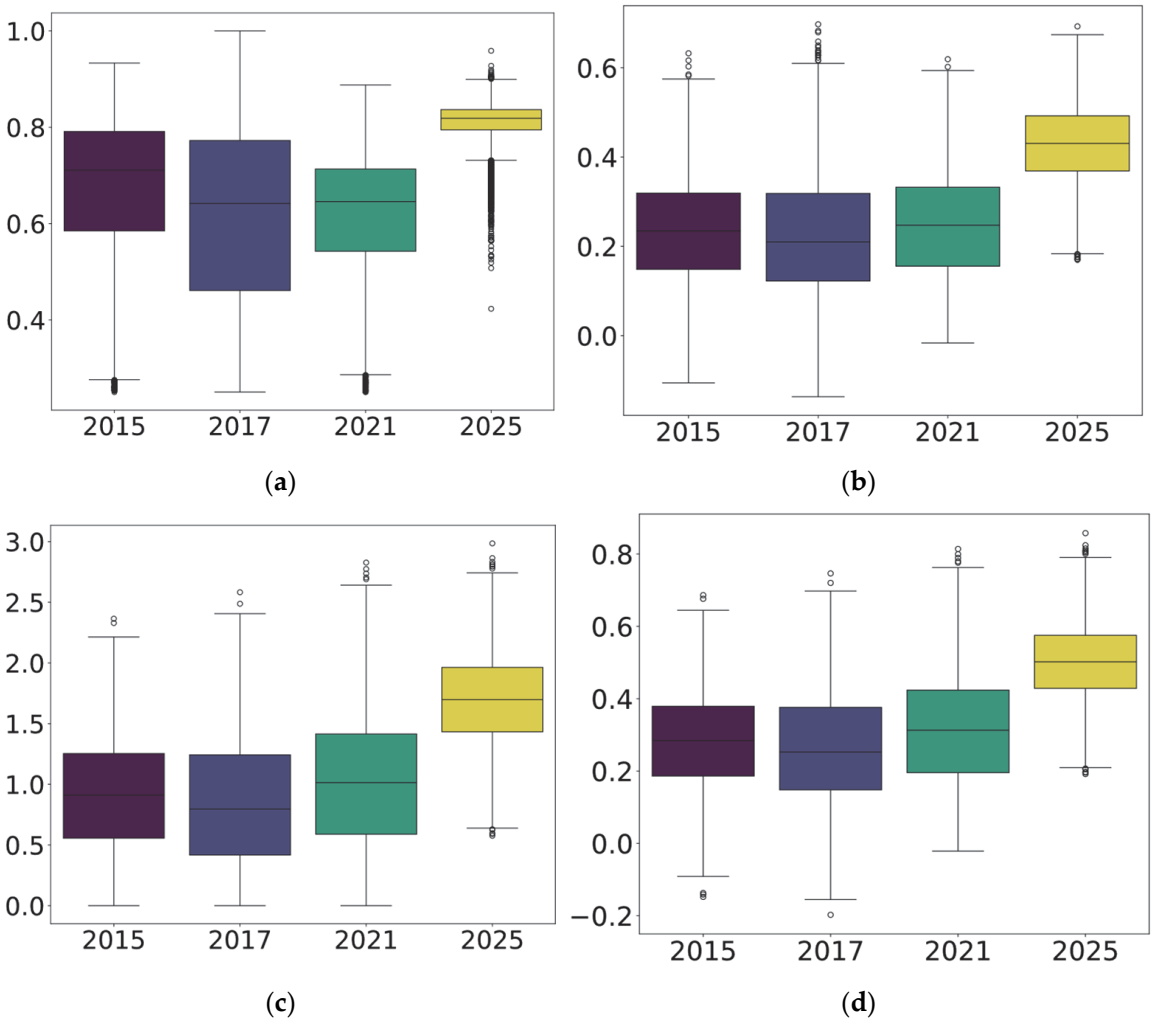

Figure 3. Box plot showing variation in vegetation indices at Unpad from 2015 to 2025: (**a**) NDVI, (**b**) MSAVI, (**c**) LAI, and (**d**) EVI.

The spatial distribution of LAI across the study area underwent a substantial transformation over the 2015–2025 observation period (Figure 4). The LAI maps use a colour scale that runs from pale blue at the lowest values (0) to dark teal-green at the highest (3.5). Masked non-vegetation surfaces, including buildings, roads, and water bodies, are shown in white and were excluded from the analysis. The pattern of LAI matched the land-use zoning of the study area closely. The densest and most continuous canopy was found in the Ciparanje Area to the north and the Arboretum Area to the southwest. In contrast, the Academic Building Area in the central-to-southern part was mostly masked, with only thin strips of vegetation remaining along its streets and courtyards. The embung in the central part of the site was also excluded as open water. The temporal trend was equally clear. In 2015, the vegetated zones, particularly Ciparanje and the Arboretum, were dominated by pale to light-blue shades, which indicate a relatively sparse canopy. These tones deepened to medium blue through 2017 and 2021 as leaf area increased across both zones. By 2025, most of the vegetated surface had turned darker teal-blue and was spread more evenly, giving the highest and most uniform LAI of all the years observed. This gradual darkening of the blue points to a clear gain in canopy density and greenness between 2015 and 2025,

with Ciparanje and the Arboretum forming the green core of the campus and holding most of its leaf area throughout the period.

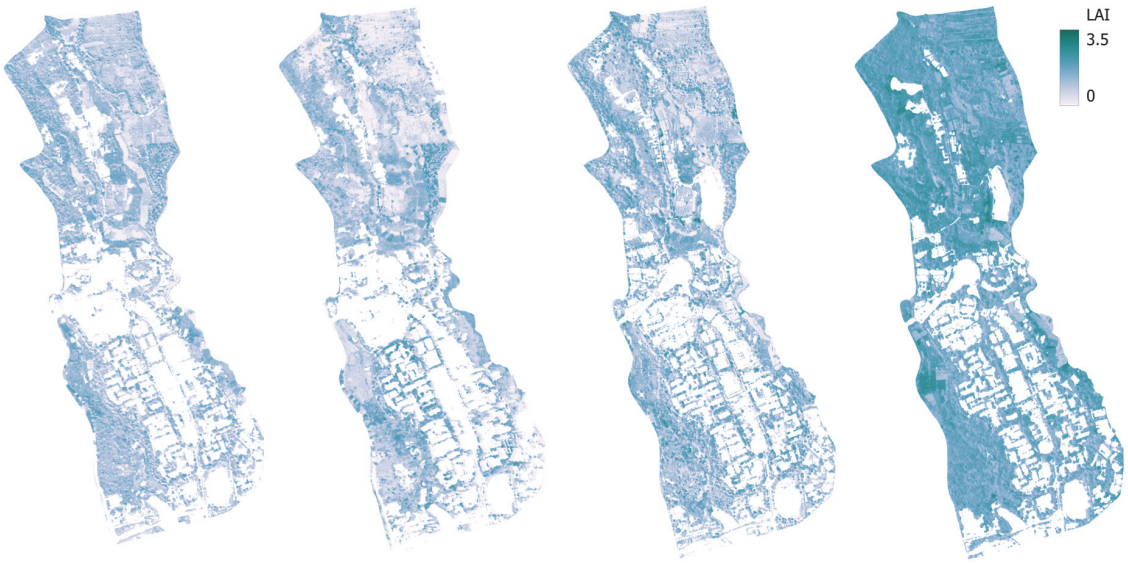

Figure 4. Spatial distribution of leaf area index (LAI) across Unpad: (**a**) 2015, (**b**) 2017, (**c**) 2021, and (**d**) 2025.

3.2. Temporal and Spatial AGB_0 Value

AGB_0 represents the amount of biomass stored in vegetation. The temporal trend in median AGB_0 values follows a pattern consistent with that of the vegetation. The AGB_0 values across the study area increased progressively over the 2015–2025 observation period, as illustrated in Figure 5. The AGB_0 values across the study area increased progressively over the 2015–2025 observation period, with their median values increasing from 0.326 in 2015 to 0.431 in 2025. A slight decline in 2017 (0.311) preceded a steady rise through 2021 (0.340) and a pronounced increase in 2025. The interquartile range narrowed in the final year (from 0.110 in 2021 to 0.071 in 2025), indicating that biomass became not only higher but also more spatially uniform as the canopy matured. This highlights spatial heterogeneity in vegetation structure, which may persist despite overall biomass growth. These findings are consistent with the spatiotemporal recovery of vegetation cover identified in the LAI analysis, collectively suggesting a sustained increase in carbon stock throughout the observation period.

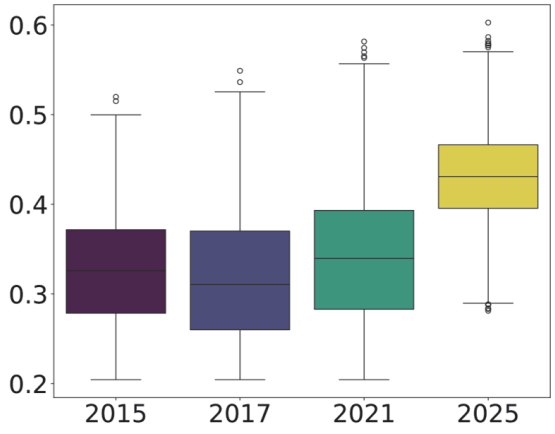

Figure 5. Box plot showing variation in AGB_0 in ton/pixel at Unpad from 2015 to 2025.

The spatial distribution of AGB_0, presented in Figure 6, clearly illustrates the temporal dynamics of biomass across Unpad. The AGB_0 maps use a colour scale that runs from yellow at the lowest values (0) to dark red-maroon at the highest (0.6713). Overall, AGB_0 increases progressively from 2015 to 2025. As with LAI, the distribution of biomass matched the land-use zoning of the study area. Deep red dominated the vegetated zones every year, and the Ciparanje Area to the north and the Arboretum Area to the southwest held the most extensive and continuous high-biomass cover. The Academic Building Area in the central-to-southern part was mostly masked, with only narrow vegetated strips between the buildings, and the embung was excluded as open water. The temporal trend was equally clear. The main departure from the otherwise stable pattern occurred in 2017, when scattered orange-to-yellow patches appeared within the Ciparanje Area, marking pockets of lower biomass. These lighter patches had largely disappeared by 2025, when the deep-red cover across Ciparanje and the Arboretum became more continuous and even. This gives the widest and most uniform biomass distribution of all the years observed, with Ciparanje and the Arboretum holding most of the area's above-ground biomass throughout the period.

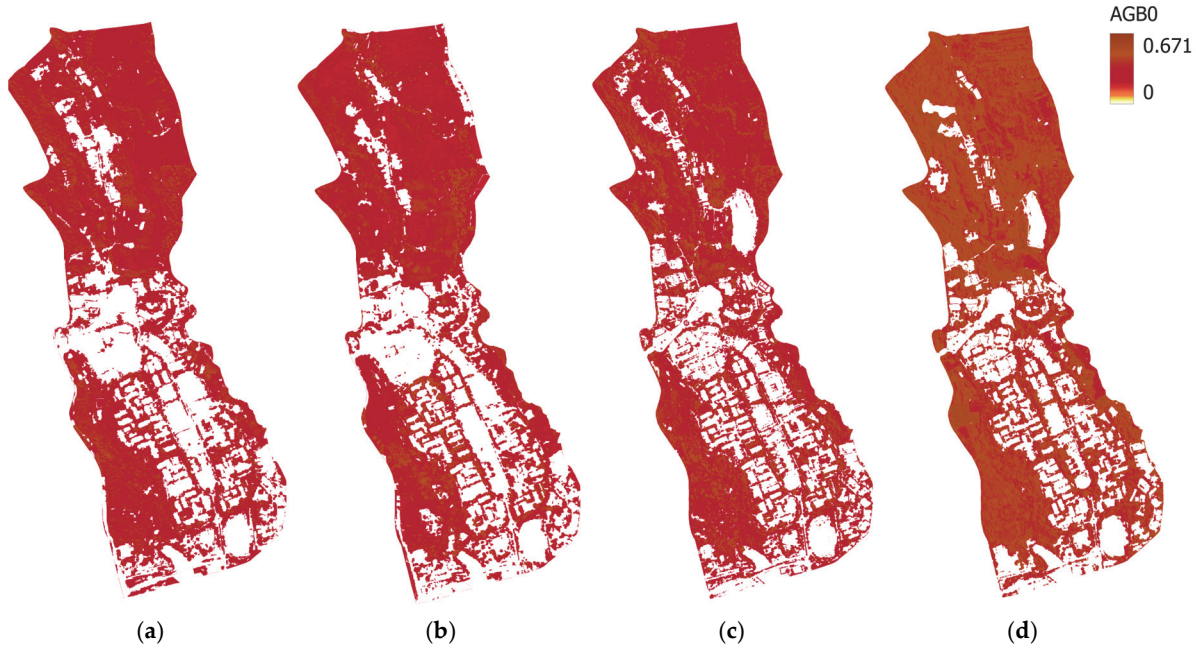

Figure 6. Spatial distribution of AGB_0 values (tonnes/pixel) across Unpad: (**a**) 2015, (**b**) 2017, (**c**) 2021, and (**d**) 2025.

3.3. AGB Modelling Using Vegetation Indices

To develop an improved AGB estimation model, each vegetation index was plotted against the estimated AGB_0 values. In this framework, the vegetation indices were treated as independent variables x, while the estimated AGB_0 served as the dependent variable (y). LAI and EVI indices were excluded from this analysis because they were already incorporated into the initial AGB_0 model. Each remaining vegetation index (NDVI, MSAVI, RGR) was regressed against AGB_0 as a simple linear model. MSAVI achieved the highest R^2 in every year (0.991 in 2015, 0.987 in 2017, 0.998 in 2021, and 0.992 in 2025), well above NDVI (0.132 to 0.780) and RGR (0.019 to 0.471), and was therefore selected as the final AGB model. Intercept (a), slope (b) and R^2 values for the three indices are summarised in Table 4.

Table 4. Model coefficients and R-square values with high-resolution remote sensing data to predict AGB.

Index	2015			2017			2021			2025		
	a	b	R^2	a	b	R^2	a	b	R^2	a	b	R^2
MSAVI	0.200	0.529	0.991	0.201	0.520	0.987	0.187	0.622	0.988	0.183	0.578	0.993
RGR	0.521	−0.204	0.458	0.321	−0.005	0.019	0.546	−0.227	0.458	0.652	−0.275	0.472
NDVI	0.172	0.241	0.648	0.200	0.225	0.780	0.133	0.348	0.532	0.108	0.398	0.132

For the selected MSAVI model, adjusted R^2 matched R^2 to three decimal places (0.991, 0.987, 0.988, and 0.993 for 2015, 2017, 2021, and 2025, respectively). RMSE ranged from 0.004 to 0.008 tonnes/pixel, MAE from 0.003 to 0.006 tonnes/pixel, and MAPE from 0.76% to 2.07%. The regression was significant at $p < 0.001$ in every year, as confirmed by both the F-test and the *t*-test of the slope coefficient; the Durbin–Watson statistic stayed within 1.974–2.013, indicating no residual autocorrelation. The slope coefficient varied only between 0.520 (2017) and 0.622 (2021) within tight 95% confidence intervals, confirming strong stability across the four years. K-fold cross-validation (k = 5) reproduced the in-sample fit (R^2 = 0.987–0.993), indicating no overfitting. Full diagnostics are reported in Table 5.

Table 5. Model selected diagnostics and cross-validation results.

Year	R^2	adj R^2	RMSE	MAE	MAPE (%)	F	DW	K-Fold R^2 (Mean ± SD)
2015	0.991	0.991	0.006	0.005	1.45	7.46×10^5	1.99	0.991 ± 0.0007
2017	0.987	0.987	0.008	0.006	2.07	5.35×10^5	1.97	0.987 ± 0.0007
2021	0.988	0.988	0.008	0.006	1.63	5.93×10^5	2.01	0.988 ± 0.0002
2025	0.993	0.993	0.004	0.003	0.76	9.86×10^5	2.01	0.993 ± 0.0004

The final AGB estimation equations derived from the multiple regression analysis are presented as follows in Table 6.

Table 6. Model coefficients for new AGB models.

Year	Sensor	Models Equation	
2025	WV-2	AGB = 0.200 + 0.529MSAVI	(9)
2021	WV-2	AGB = 0.201 + 0.520MSAVI	(10)
2017	WV-3	AGB = 0.187 + 0.622MSAVI	(11)
2015	WV Legion 3	AGB = 0.182 + 0.578MSAVI	(12)

To validate the developed AGB model, it was applied to predict AGB using Landsat 8 imagery acquired at the same location and during the same observation periods for cross-sensor validation. A linear regression approach was employed, with AGB derived from high-resolution satellite imagery as the independent variable (x) and AGB estimated from Landsat 8 as the dependent variable (y). The regression results are presented in Figure 7. The coefficients of determination (R^2) for 2025, 2021, 2017, and 2015 are 0.0.667, 0.246, 0.490, and 0.546, respectively. These values indicate a moderate level of agreement between AGB estimates derived from high-resolution imagery and those from Landsat 8. The variation in R^2 across years suggests that consistency between datasets is not uniform, with stronger agreement in 2025 and weaker in earlier years. These differences are likely influenced by sensor-specific characteristics at the time of image acquisition. Overall, the results indicate that while Landsat 8 data can provide a general representation of biomass patterns, high-resolution imagery captures spatial variability more effectively, particularly in heterogeneous landscapes such as campus environments. Differences in

spatial resolution and spectral sensitivity between the datasets likely contribute to the observed discrepancies, although the moderate correlation confirms that both datasets exhibit comparable trends in AGB distribution.

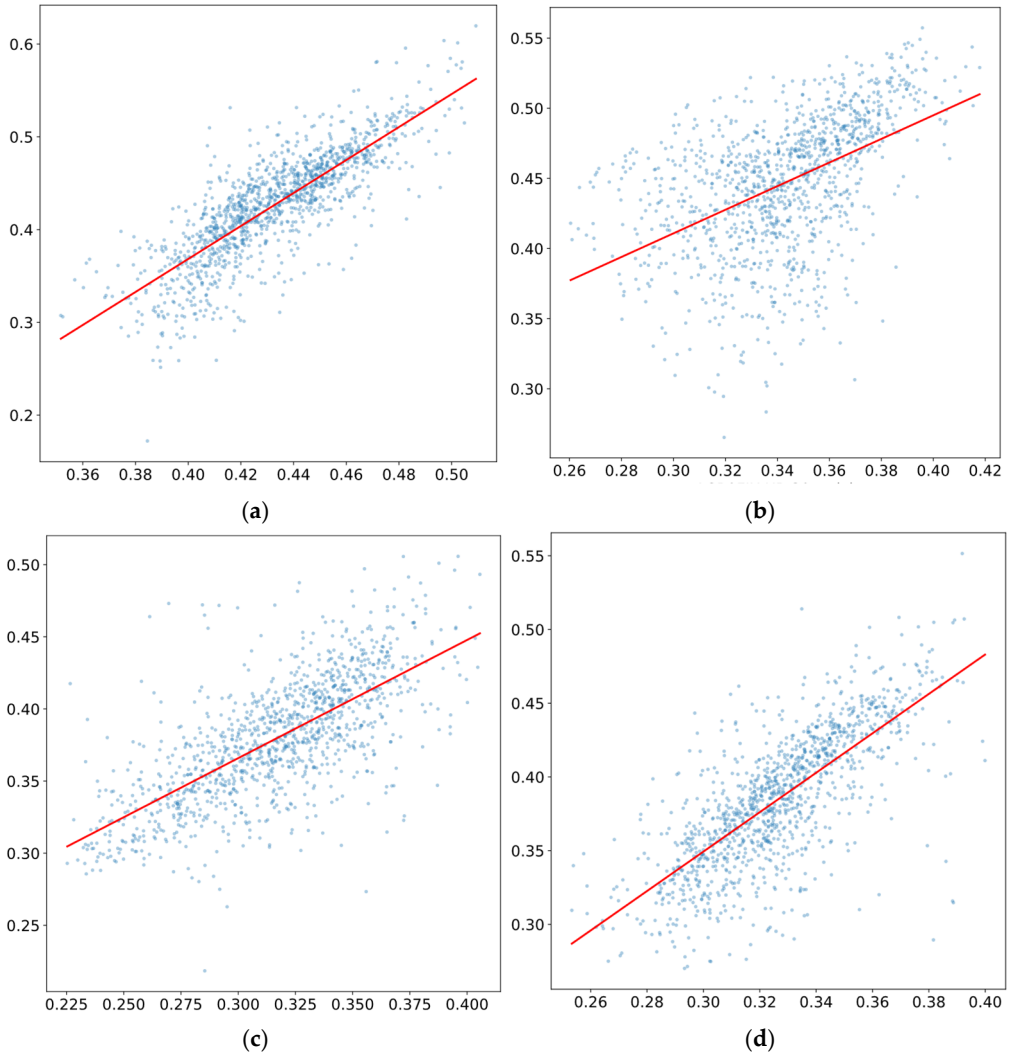

Figure 7. Scatter plots comparing AGB estimates derived from Landsat 8 and high-resolution satellite imagery: (**a**) Landsat 8 vs. Legion-03 (2025), (**b**) Landsat 8 vs. WorldView-3 (2021), (**c**) Landsat 8 vs. WorldView-2 (2017), and (**d**) Landsat 8 vs. WorldView-3 (2015).

3.4. Temporal and Spatial Carbon-Stock Value

Carbon stock was estimated by multiplying AGB values by a carbon conversion factor of 0.5. The average carbon-stock values for 2015, 2017, 2021, and 2025 are 20.381 tonnes/ha, 19.754 tonnes/ha, 22.281 tonnes/ha, and 29.160 tonnes/ha, respectively, with a substantial increase in 2025. The carbon-stock values across the study area exhibited a progressive stabilisation trend over the 2015–2025 observation period, as seen in Figure 8. In 2015, the median distribution reflected high spatial heterogeneity in carbon stocks, attributable to the fragmented vegetation cover characteristic of this period. A marginal decline in median value was observed in 2017, suggesting continued spatial variability in carbon accumulation. By 2021, both the outlier magnitude and distribution spread contracted considerably, indicative of a more spatially homogeneous carbon-stock landscape consistent with the progressive vegetation recovery identified in the LAI and AGB analyses. The 2025 distribution demonstrated the most stabilised pattern across all observed years, suggesting a landscape-wide convergence toward more uniform and marginally improved carbon-

stock accumulation. Collectively, these findings indicate that the study area underwent a sustained transition from a spatially heterogeneous, disturbance-driven carbon stock regime in 2015 to a more ecologically stable, spatially consistent carbon accumulation pattern by 2025.

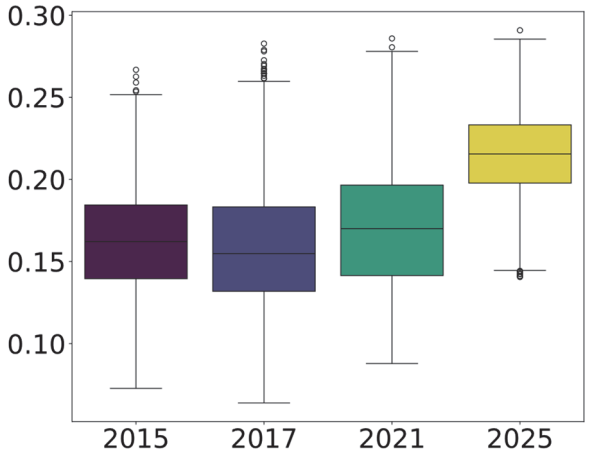

Figure 8. Box plot showing variation in carbon stock in tonnes/pixel at Unpad from 2015 to 2025.

The spatial distribution of carbon stock is presented in Figure 9. The spatial distribution of carbon stocks across the study area showed a gradual improvement over the 2015–2025 observation period. In 2015 and 2017, the vegetated zones carried a mix of medium-green and yellow-green tones, with the lighter, lower-carbon patches most visible across Ciparanje in 2017. The green deepened from 2021 onward, and by 2025, both Ciparanje and the Arboretum had turned almost uniformly dark green, giving the highest and most evenly spread carbon stock of all the years observed. This gradual shift toward darker green points to a steady increase in carbon storage between 2015 and 2025, with Ciparanje and the Arboretum forming the green core of the campus and holding most of its carbon throughout the period. Collectively, these findings indicate a sustained landscape-scale transition from a heterogeneous, low-carbon stock in 2015 to a more homogeneous, high-carbon stock distribution by 2025, corroborating the positive trajectories identified in both the LAI and AGB analyses throughout the observation period.

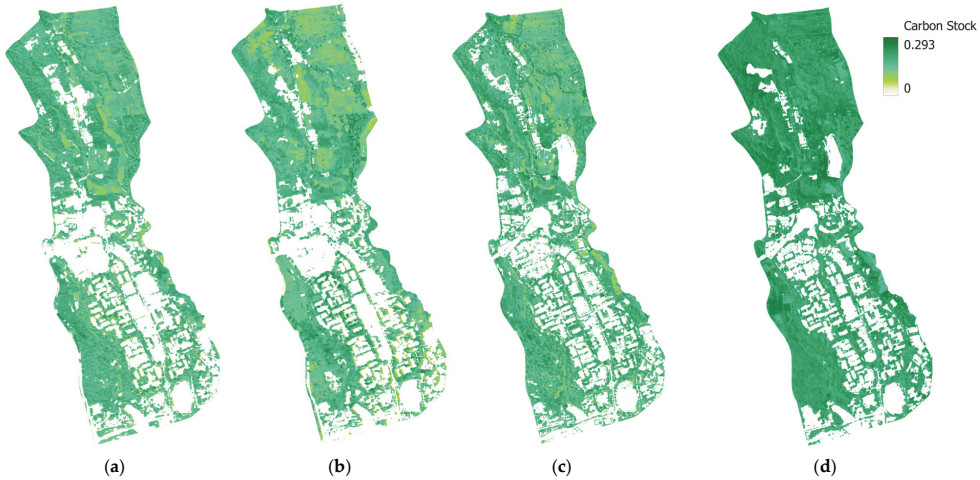

Figure 9. Spatial distribution of carbon stock (tonnes/pixel) across the Unpad area: (**a**) 2015, (**b**) 2017, (**c**) 2021, and (**d**) 2025.

4. Discussion

4.1. Index-Based Characterisation of Unpad

Based on the results, EVI, LAI, and MSAVI show a consistent increasing trend from 2015 to 2025, indicating a substantial expansion of canopy cover within the Unpad area. NDVI increased from 0.711 to 0.819, although its interquartile range narrowed considerably from 0.206 to 0.042. This contraction suggests that NDVI began to saturate as the canopy closed, reducing its ability to distinguish dense vegetation in the later years. EVI, in contrast, increased from 0.284 to 0.502 while retaining a broad distribution, confirming that it remained sensitive in densely vegetated areas where NDVI levelled off. MSAVI showed a similar upward trend, rising from 0.234 to 0.431, but with a stable spread across all years. This narrow and consistent distribution indicates that MSAVI was largely unaffected by soil background effects, which is the main reason it was selected as the principal predictor in the AGB model. The most pronounced change was observed in LAI, whose median nearly doubled from 0.911 to 1.698, consistent with the increasing leaf density and structural complexity of the canopy over the decade.

Furthermore, MSAVI provides a reliable approach for vegetation analysis in heterogeneous environments. It is a modified version of the original soil-adjusted vegetation index (SAVI) [13], improved through a self-adjusting soil-correction factor that adapts to local canopy and soil conditions [14]. This design effectively reduces soil background interference while preserving sensitivity to canopy structure, an advantage that is also reported in previous reviews of vegetation indices [17,48]. These characteristics are particularly important in heterogeneous environments such as the Unpad campus, where the proportion of exposed soil, paved surfaces, and built-up areas varies substantially across the landscape and where accurate differentiation of vegetation conditions is required [49]. MSAVI is also less affected by the saturation effects that commonly occur in broadband indices such as NDVI under dense canopy conditions [19]. Previous studies have shown that this property translates into better AGB estimation compared to NDVI in heterogeneous urban Arboretum settings [16], and more generally, that soil-adjusted indices outperform soil-unadjusted indices for above-ground green biomass estimation across various vegetation cover types [50]. The stable distribution of MSAVI observed across the WorldView and Legion acquisitions also suggests that the index is not sensitive to minor inter-sensor radiometric differences.

4.2. Modelling Aboveground Biomass

Among the three vegetation indices tested (NDVI, MSAVI, RGR), MSAVI consistently achieved the highest coefficient of determination with AGB across the four acquisition years, with R^2 values ranging from 0.987 to 0.993 (Table 4). NDVI produced R^2 values between 0.132 and 0.780 and RGR between 0.019 and 0.471, indicating that MSAVI provides the most informative single predictor of AGB in this study. The advantage of MSAVI is attributable to its self-adjusting soil-correction term, which minimises the influence of the soil background on the vegetation signal. NDVI is known to be unstable in scenes with exposed soil because variations in soil colour, brightness, and moisture produce red–NIR contrasts that are unrelated to canopy biomass; the soil-adjusted vegetation index (SAVI) corrects for this effect through a fixed adjustment factor, while MSAVI derives the factor directly from the image data and therefore adapts to the variable proportion of exposed soil across the scene. MSAVI is also less susceptible than NDVI to saturation in dense canopies, allowing it to discriminate biomass differences in the more vegetated parts of the mosaic. These properties make MSAVI particularly well suited to mixed-species and mixed-cover landscapes. Comparable performance has been reported by Thinley et al. [16]

in a subtropical urban Arboretum, by Forkuor et al. [20] in West African drylands, and by Pandit et al. [51] in subtropical community forests.

The accuracy and stability diagnostics support this choice. RMSE ranged from 0.004 to 0.008 tonnnes/pixel, MAE from 0.003 to 0.006 tonnes/pixel, and MAPE from 0.76% to 2.07% across the four years, representing low error for vegetation-index-based AGB estimation. The adjusted R^2 matched R^2 in every year; all regressions were significant at $p < 0.001$, and the Durbin–Watson statistic stayed within 1.97–2.01, indicating no residual autocorrelation. RMSE and MAE are reported jointly because each metric describes a complementary aspect of the prediction error distribution [52]. K-five-fold cross-validation reproduced the in-sample R^2 (0.987–0.993) with standard deviations below 0.0007, giving no evidence of over-fitting and confirming that the model is consistent from year to year. Collectively, these diagnostics conform to the validation framework recommended for remote-sensing regression in heterogeneous landscapes [53] and support the interpretation that the high R^2 reflects a genuine structural relationship between MSAVI and AGB.

Across the four years, the resulting models showed stable coefficients, with the intercept (a) ranging from 0.182 to 0.202 and the slope (b) from 0.529 to 0.622. This stability indicates that the annual AGB maps, along with the carbon-stock layers derived from the satellite data, form a temporally consistent series suitable for analysing the spatial and temporal dynamics of carbon stocks across the Unpad campus.

Model performance declined substantially when projected onto Landsat 8 OLI imagery. After area-weighted resampling of the high-resolution AGB to the 30 m grid, the per-pixel regression yielded R^2 values between 0.246 and 0.667 across years. This decline does not reflect a deficiency in the MSAVI model itself but rather two distinct cross-sensor effects. The first is the mixed-pixel effect: each 30 m Landsat 8 pixel aggregates radiometric contributions from canopy, understory, and impervious surfaces, attenuating the MSAVI signal that underpins the AGB estimate. An offset of similar magnitude has been reported by Gu and Congalton [54] for biomass comparisons among PlanetScope, Sentinel-2, and Landsat 8 over heterogeneous landscapes. The second is the difference in spectral band centres and bandwidths between Landsat 8 OLI and the commercial high-resolution sensors used here, which propagates through MSAVI into the derived AGB estimate. This effect has been quantified by Astola et al. [55] for Sentinel-2 versus Landsat 8 and documented more broadly in the Landsat cross-sensor continuity literature [56]. The MSAVI–AGB equations developed in this study are therefore reliable at sub-metre resolution but cannot be transferred directly to Landsat-class imagery without sensor-specific recalibration. This limitation, together with the absence of in situ biomass measurements at the Unpad campus area required for absolute-scale validation, represents the principal limitation of the present study. Future work will address both, including the development of sensor-specific MSAVI normalisation coefficients to extend the MSAVI–AGB framework to medium-resolution imagery for landscape-scale carbon monitoring in tropical Indonesia [57,58].

4.3. Analysis, Spatial and Temporal Carbon-Stock Unpad

Carbon stock was estimated by multiplying the carbon conversion factor by AGB values derived from the newly developed model based on high-resolution satellite imagery. The results indicate a consistent increase in carbon stock within the Unpad area from 2015 to 2025, but there was a decline in 2017. This is relevant to a study conducted by Dharmawan et al. [38] regarding Unpad's urban green space, where there was a 12.71% decrease in vegetation area from 2015 to 2017. The most substantial increase is observed in 2025, with an average carbon-stock value reaching 29.160 tonnes/ha.

This upward trend in carbon stock is directly proportional to increases in AGB, vegetation indices reflecting enhanced vegetation growth and biomass accumulation across the

study area. The increase in carbon stock is also consistent with the expansion of vegetation cover within the campus. In 2015, the combined area of dense and sparse vegetation was 1,243,174 m^2 (68.69%), increasing to 1,348,497 m^2 (74.69%) in 2025. The most notable growth occurred in sparse vegetation, which expanded from 732,570 m^2 (40.59%) in 2015 to 803,243 m^2 (44.49%) in 2025. This was followed by an increase in dense vegetation, from 459,702 m^2 (25.48%) in 2017 to 545,254 m^2 (30.20%) [27].

This increase is strongly supported by large-scale tree-planting initiatives undertaken by Unpad, as reported by the campus sustainability and environmental safety unit. A continuous tree-planting programme was implemented from 2016 to 2026. Between 2016 and 2017, approximately 4936 trees were planted in academic building areas, dominated by fast-growing legumes and native hardwoods. This was followed by the planting of 268 trees of mixed hardwood and fruit-tree species in the Ciparanje Area during 2017–2018, and 950 trees in academic zones during 2018–2019, including a substantial share of coffee and mixed fruit-tree seedlings. Additional planting activities were carried out between 2020 and 2021, with 175 trees planted around the rectorate area and 100 ornamental shade trees added in academic zones during 2021–2022. Subsequent efforts included the planting of 301 fruit-tree seedlings in the embung (retention pond) area, and most recently, 200 trees were planted in 2025 in the northern and southern embung zones [26]. Tropical fast-growing legumes have been shown to accumulate above-ground carbon at high rates, reaching stocks of 193–314 tonnes per hectare in 3–6-year-old stands [59], while mature Indonesian fruit-tree collections store tens to more than one hundred Mg C per hectare [60]. Slower-growing native hardwoods develop high per-tree carbon densities that account for much of the legacy biomass observed in the Arboretum [61]. These findings highlight the significant impact of sustained greening programmes on increasing vegetation cover, biomass accumulation, and carbon sequestration within an urban campus environment.

Based on Figure 9, the spatial distribution of carbon stocks indicates that the highest values are concentrated in the northern part of the campus and the Arboretum. These areas serve as research zones encompassing campus biodiversity, as well as experimental land and plantation sites. The average carbon stock in these areas is recorded at 8.602 tonnes/ha and 2.612 tonnes/ha in 2025, respectively. The remaining zones, including the academic precinct and the embung (retention pond) catchment, have been the focus of progressive institutional reforestation since 2016; the embung surroundings in particular were left with bare and degraded soils after pond construction and have since been intensively replanted, accounting for much of the 2017–2025 increase observed at the campus mean. The campus vegetation is predominantly planted rather than natural, with only fragmentary natural phytocenoses potentially preserved at the northern margin [62].

The carbon-stock estimate of 2.293 tonnes/ha obtained from remote sensing in this study is comparable to the value of 2.10 tonnes/ha reported by Aswada et al. [25] for the Arboretum area. Their study estimated carbon stock in July 2022 using non-destructive sampling and the pantropical allometric equation across five land-use types within the Arboretum. The small difference between the two values can be attributed to the different estimation methods and the different time of data acquisition. However, the two results are still in good agreement, indicating that the remote sensing approach used in this study can be applied to estimate carbon stock across the Unpad campus area as a practical alternative to field-based inventory.

When compared with other campus-scale studies, the Unpad mean of 29.16 t C/ha exceeds the 19.7 t C/ha reported by Lavista et al. [62] for IPB Darmaga in Bogor, while remaining lower than the 46.77 t C/ha weighted mean reported by Anantsuksomsri et al. [24] for six universities in the Bangkok Metropolitan Region, where the difference is mainly attributable to site geometry and reporting convention rather than to climate. The val-

ues of 23–27 t C/ha reported by Vicharnakorn et al. [23] for Savannakhet, Lao PDR, and 28–35 t C/ha obtained by Thinley et al. [16] for a sub-tropical Arboretum in Queensland indicate that Unpad falls within the upper portion of comparable tropical and sub-tropical campuses, exceeding the Savannakhet range and approaching the lower bound of the Queensland range. The Indian literature reflects a wider spectrum: 5–8 t C/ha were reported for Maharshi Dayanand University, Rohtak [63] and Amity University, Noida [22] in drier sub-tropical settings, both of which Unpad exceeds by a factor of four to five, whereas Cotton University, Guwahati [64] recorded 346 Mg C ha^{-1} for a small, densely planted footprint that lies well outside the typical campus range. The estimated annual sequestration rate of 0.88 t C/ha/yr at Unpad over 2015–2025 likely reflects the combined influence of the tropical climate and the sustained planting programmes implemented over the past decade and points to the central role of management decisions in shaping the future evolution of the campus carbon stock.

4.4. Implications of Carbon Stock for Campus Sustainability Management

The 2025 campus-mean carbon stock of 29.160 tonnes/ha provides a quantitative baseline for sustainability management at the Unpad Jatinangor Campus. The largest share of the stock is concentrated in the Northern Ciparanje Area and the Western Arboretum, consistent with urban-forest studies in which a small number of mature trees and dense patches hold the majority of the carbon. Construction within these zones therefore has a disproportionate impact on the campus stock, and vegetation stocks have been shown to decline substantially when mature stands are removed without compensation in rapidly urbanising regions [65]. Designating both areas as no-build conservation zones, with a tree-replacement ratio calibrated to any converted footprint, can preserve the existing stock and reduce future losses. The canopy further regulates the local climate: shading and evapotranspiration attenuate the urban heat-island effect and lower the cooling-energy demand of surrounding buildings [61,65,66], and the leaf surfaces intercept particulate matter and absorb gaseous pollutants, improving local air quality [67].

At the institutional scale, the measured stock provides an empirical basis for integrating the environmental, economic, and social dimensions of campus operation. Continued growth of the stock contributes to localised climate mitigation and to habitat connectivity between the Arboretum, the Ciparanje stand, and the riparian corridor; the associated canopy-mediated cooling and air-quality benefits lower recurring operational costs and indirect emissions; and the dataset itself can be incorporated into teaching activities related to remote sensing, ecological modelling, and sustainability assessment [68,69].

These outcomes map directly to several United Nations Sustainable Development Goals (SDGs). Continued growth of the campus stock contributes to SDG 13 (Climate Action) through localised mitigation and a replicable monitoring approach for higher-education institutions. Protection of the Arboretum, the Ciparanje stand, and the riparian bamboo corridor supports SDG 15 (Life on Land) by preserving ecological corridors within a semi-urban landscape. Embedding carbon-aware planning into the campus master plan contributes to SDG 11 (Sustainable Cities and Communities), while the use of the dataset in teaching and student-participatory monitoring aligns with SDG 4 (Quality Education), particularly target 4.7 on education for sustainable development. Finally, methodological alignment with international reporting standards supports SDG 17 (Partnerships for the Goals) through collaboration with universities engaged in comparable carbon-accounting frameworks.

4.5. Study Limitations

Several limitations were identified in this study. The primary limitation lies in the validation and accuracy of the developed AGB model. The absence of field-based measurements restricts the robustness of model validation. Therefore, integrating remote sensing approaches with in situ data is recommended to improve model reliability. Field-based carbon-stock estimation can be enhanced by incorporating biophysical tree parameters, such as diameter at breast height (DBH), tree height, and wood density, which are essential for accurate aboveground biomass calculations.

Another limitation is that the developed model can only be applied to high-resolution satellite imagery (WorldView and Legion-03). When transferred to medium-resolution satellites (Landsat 8), the model is less accurate in predicting AGB and requires radiometric adjustment of the sensor.

5. Conclusions

This study aimed to estimate and analyse the temporal and spatial distribution of carbon stock in the Unpad area using high-resolution remote sensing imagery. The results indicate a consistent increase in carbon stock from 2015 to 2025. The average carbon stock values for 2015, 2017, 2021, and 2025 were 20.381 tonnes/ha, 19.754 tonnes/ha, 22.281 tonnes/ha, and 29.160 tonnes/ha, respectively, with an increase in 2025.

Carbon stock was derived from AGB estimates using a carbon conversion factor of 0.5. The improved AGB model was developed by integrating vegetation indices, MSAVI, resulting in the following year-specific models: AGB = 0.182 + 0.578 MSAVI (2025), AGB = 0.187 + 0.622 MSAVI (2021), AGB = 0.201 + 0.520 MSAVI (2017), and AGB = 0.200 + 0.529 MSAVI (2015). These models achieved high R^2 values of 0.993 (2025), 0.988 (2021), 0.987 (2017), and 0.991 (2015). The resulting carbon-stock values were also comparable to field-based measurements collected in the Arboretum area, where the remote-sensing approach yielded 2.293 tonnes/ha, and the field method yielded 2.10 tonnes/ha. The increase in AGB is strongly correlated with the rising values of vegetation indices, particularly NDVI, LAI, and EVI, indicating enhanced vegetation density and canopy structure. Furthermore, the observed increase in carbon stock is closely associated with extensive greening initiatives undertaken by the university from 2015 to 2025, which have contributed to the expansion of vegetation cover and biomass accumulation across the campus.

Author Contributions: Conceptualization, R.H., I.A.D. and M.A.; methodology, R.H., I.A.D. and M.A.; software, R.H. and B.M.; validation, I.A.D. and M.A.; formal analysis, R.H., I.A.D. and M.A.; investigation, R.H., B.M. and R.A.D.; resources, I.A.D., G.L.U.S. and B.W.; data curation, I.A.D. and M.A.; writing—original draft preparation, R.H., R.A.D. and K.S.; writing—review and editing, I.A.D. and K.S.; visualisation, R.H. and I.A.D.; supervision, I.A.D. and M.A.; project administration, R.A.D. and B.W.; funding acquisition, I.A.D. All authors have read and agreed to the published version of the manuscript.

Funding: The research was supported by Riset Penugasan Universitas (RPU) under Contract Number 1158/UN6.3.1/PT.00/2025. The publication fee was supported by Universitas Padjadjaran through the Indonesian Endowment Fund for Education (LPDP) on behalf of the Indonesian Ministry of Higher Education, Science, and Technology, and managed under the EQUITY Program (Contract Nos. 4303/B3/DT.03.08/2025 and 3927/UN6.RKT/HK.07.00/2025).

Institutional Review Board Statement: Not applicable.

Informed Consent Statement: Not applicable.

Data Availability Statement: These data are not publicly available, but may be accessed upon reasonable request.

Conflicts of Interest: The authors declare no conflicts of interest.

Abbreviations

The following abbreviations are used in this manuscript:

AGB	Above-ground biomass
EVI	Enhanced vegetation index
LAI	Leaf area index
MSAVI	Modified soil adjust vegetation index
NDVI	Normalised difference vegetation index
RGR	Red green index

References

1. Mitchard, E.T.A. The Tropical Forest Carbon Cycle and Climate Change. *Nature* **2018**, *559*, 527–534. [CrossRef] [PubMed]
2. Pan, Y.; Birdsey, R.A.; Fang, J.; Houghton, R.; Kauppi, P.E.; Kurz, W.A.; Phillips, O.L.; Shvidenko, A.; Lewis, S.L.; Canadell, J.G.; et al. A Large and Persistent Carbon Sink in the World's Forests. *Science* **2011**, *333*, 988–993. [CrossRef] [PubMed]
3. Saatchi, S.S.; Harris, N.L.; Brown, S.; Lefsky, M.; Mitchard, E.T.A.; Salas, W.; Zutta, B.R.; Buermann, W.; Lewis, S.L.; Hagen, S.; et al. Benchmark Map of Forest Carbon Stocks in Tropical Regions across Three Continents. *Proc. Natl. Acad. Sci. USA* **2011**, *108*, 9899–9904. [CrossRef] [PubMed]
4. Spawn, S.A.; Sullivan, C.C.; Lark, T.J.; Gibbs, H.K. Harmonized Global Maps of above and Belowground Biomass Carbon Density in the Year 2010. *Sci. Data* **2020**, *7*, 112. [CrossRef] [PubMed]
5. Nesha, K.; Herold, M.; De Sy, V.; Duchelle, A.E.; Martius, C.; Branthomme, A.; Garzuglia, M.; Jonsson, O.; Pekkarinen, A. An Assessment of Data Sources, Data Quality and Changes in National Forest Monitoring Capacities in the Global Forest Resources Assessment 2005–2020. *Environ. Res. Lett.* **2021**, *16*, 054029. [CrossRef]
6. Friedlingstein, P.; O'Sullivan, M.; Jones, M.W.; Andrew, R.M.; Gregor, L.; Hauck, J.; Le Quéré, C.; Luijkx, I.T.; Olsen, A.; Peters, G.P.; et al. Global Carbon Budget 2022. *Earth Syst. Sci. Data* **2022**, *14*, 4811–4900. [CrossRef]
7. Lamahewage, S.H.G.; Witharana, C.; Riemann, R.; Fahey, R.; Worthley, T. Aboveground Biomass Estimation Using Multimodal Remote Sensing Observations and Machine Learning in Mixed Temperate Forest. *Sci. Rep.* **2025**, *15*, 31120. [CrossRef] [PubMed]
8. Dubayah, R.; Blair, J.B.; Goetz, S.; Fatoyinbo, L.; Hansen, M.; Healey, S.; Hofton, M.; Hurtt, G.; Kellner, J.; Luthcke, S.; et al. The Global Ecosystem Dynamics Investigation: High-Resolution Laser Ranging of the Earth's Forests and Topography. *Sci. Remote Sens.* **2020**, *1*, 100002. [CrossRef]
9. Huete, A.; Didan, K.; Miura, T.; Rodriguez, E.P.; Gao, X.; Ferreira, L.G. Overview of the Radiometric and Biophysical Performance of the MODIS Vegetation Indices. *Remote Sens. Environ.* **2002**, *83*, 195–213. [CrossRef]
10. Almeida-Ñauñay, A.F.; Tarquis, A.M.; López-Herrera, J.; Pérez-Martín, E.; Pancorbo, J.L.; Raya-Sereno, M.D.; Quemada, M. Optimization of Soil Background Removal to Improve the Prediction of Wheat Traits with UAV Imagery. *Comput. Electron. Agric.* **2023**, *205*, 107559. [CrossRef]
11. Wulder, M.A.; Coops, N.C.; Roy, D.P.; White, J.C.; Hermosilla, T. Land Cover 2.0. *Int. J. Remote Sens.* **2018**, *39*, 4254–4284. [CrossRef]
12. Santoro, M.; Cartus, O.; Carvalhais, N.; Rozendaal, D.M.A.; Avitabile, V.; Araza, A.; de Bruin, S.; Herold, M.; Quegan, S.; Rodríguez-Veiga, P.; et al. The Global Forest Above-Ground Biomass Pool for 2010 Estimated from High-Resolution Satellite Observations. *Earth Syst. Sci. Data* **2021**, *13*, 3927–3950. [CrossRef]
13. Huete, A.R. A Soil-Adjusted Vegetation Index (SAVI). *Remote Sens. Environ.* **1988**, *25*, 295–309. [CrossRef]
14. Qi, J.; Chehbouni, A.; Huete, A.R.; Kerr, Y.H.; Sorooshian, S. A Modified Soil Adjusted Vegetation Index. *Remote Sens. Environ.* **1994**, *48*, 119–126. [CrossRef]
15. Huete, A.R.; Liu, H.Q.; Batchily, K.; Van Leeuwen, W. A Comparison of Vegetation Indices over a Global Set of TM Images for EOS-MODIS. *Remote Sens. Environ.* **1997**, *59*, 440–451. [CrossRef]
16. Thinley, J.; Pickering, C.; Ndehedehe, C. Using Vegetation and Chlorophyll Indices to Model above Ground Biomass over Time in an Urban Arboretum in Subtropical Queensland. *Remote Sens. Appl.* **2024**, *34*, 101202. [CrossRef]
17. Xue, J.; Su, B. Significant Remote Sensing Vegetation Indices: A Review of Developments and Applications. *J. Sens.* **2017**, *2017*, 1353691. [CrossRef]
18. Lu, D. The Potential and Challenge of Remote Sensing-based Biomass Estimation. *Int. J. Remote Sens.* **2006**, *27*, 1297–1328. [CrossRef]
19. Mutanga, O.; Skidmore, A.K. Narrow Band Vegetation Indices Overcome the Saturation Problem in Biomass Estimation. *Int. J. Remote Sens.* **2004**, *25*, 3999–4014. [CrossRef]
20. Forkuor, G.; Benewinde Zoungrana, J.-B.; Dimobe, K.; Ouattara, B.; Vadrevu, K.P.; Tondoh, J.E. Above-Ground Biomass Mapping in West African Dryland Forest Using Sentinel-1 and 2 Datasets—A Case Study. *Remote Sens. Environ.* **2020**, *236*, 111496. [CrossRef]

21. Muhe, S.; Argaw, M. Estimation of Above-Ground Biomass in Tropical Afro-Montane Forest Using Sentinel-2 Derived Indices. *Environ. Syst. Res.* **2022**, *11*, 5. [CrossRef]
22. Sharma, R.; Pradhan, L.; Kumari, M.; Bhattacharya, P. Assessment of Carbon Sequestration Potential of Tree Species in Amity University Campus Noida. *Environ. Sci. Proc.* **2021**, *3*, 52.
23. Vicharnakorn, P.; Shrestha, R.P.; Nagai, M.; Salam, A.P.; Kiratiprayoon, S. Carbon Stock Assessment Using Remote Sensing and Forest Inventory Data in Savannakhet, Lao PDR. *Remote Sens.* **2014**, *6*, 5452–5479. [CrossRef]
24. Anantsuksomsri, S.; Positlimpakul, K.; Chatakul, P.; Janpathompong, D.; Chen, G.; Tontisirin, N. Carbon Sequestration Analysis of the University Campuses in the Bangkok Metropolitan Region. *J. Infrastruct. Policy Dev.* **2024**, *8*, 2153579. [CrossRef]
25. Aswada, V.S.; Kusmoro, J.; Ilmi, F.; Butarbutar, C.L.; Rahmawati, D.; Zahra, E.; Rahmah, L.A.; Septiya, C.A.; Hidayati, U.R.A. Estimasi Simpanan Karbon Pada Vegetasi Pohon di Beberapa Tipe Penggunaan Lahan Arboretum Universitas Padjadjaran. *Biotika* **2023**, *21*, 59–67. [CrossRef]
26. Center for Sustainable Campus Development and Envrionmental Safety. *Universitas Padjadjaran Tree Planting and Greening Report*; Center for Sustainable Campus Development and Envrionmental Safety: Sumedang, Indonesia, 2025.
27. Midad, B.; Hanafi, R.; Aufaristama, M.; Dharmawan, I.A. Object-Based Random Forest Approach for High-Resolution Mapping of Urban Green Space Dynamics in a University Campus. *Appl. Sci.* **2025**, *15*, 13183. [CrossRef]
28. Desenaldo, R.A.; Azis, A.M.; Anastasia, I.L.; Sinaga, Y.; Dharmawan, I.A. Remote Sensing and Cloud Computing Applications for Mapping Cereal Foodstuffs Agricultural Land in East Kalimantan, Indonesia. *AIP Conf. Proc.* **2023**, *2858*, 040003. [CrossRef]
29. Chavez, P.S. An Improved Dark-Object Subtraction Technique for Atmospheric Scattering Correction of Multispectral Data. *Remote Sens. Environ.* **1988**, *24*, 459–479. [CrossRef]
30. Hill, V.J.; Zimmerman, R.C.; Bissett, P.; Kohler, D.; Schaeffer, B.; Coffer, M.; Li, J.; Islam, K.A. Impact of Atmospheric Correction on Classification and Quantification of Seagrass Density from WorldView-2 Imagery. *Remote Sens.* **2023**, *15*, 4715. [CrossRef] [PubMed]
31. Pancorbo, J.L.; Lamb, B.T.; Quemada, M.; Hively, W.D.; Gonzalez-Fernandez, I.; Molina, I. Sentinel-2 and WorldView-3 Atmospheric Correction and Signal Normalization Based on Ground-Truth Spectroradiometric Measurements. *ISPRS J. Photogramm. Remote Sens.* **2021**, *173*, 166–180. [CrossRef]
32. Wicaksono, P.; Hafizt, M. Dark Target Effectiveness for Dark-object Subtraction Atmospheric Correction Method on Mangrove Above-ground Carbon Stock Mapping. *IET Image Process.* **2018**, *12*, 582–587. [CrossRef]
33. Zhang, Y.; Wang, X.; Tan, H.; Xu, C.; Ma, X.; Xu, T. Region Merging Method for Remote Sensing Spectral Image Aided by Inter-Segment and Boundary Homogeneities. *Remote Sens.* **2019**, *11*, 1414. [CrossRef]
34. Hua, S.; Jin, S.; Song, Z.; Liu, X. Geometric Correction of Meteorological Satellite Cloud Image Data Position under Multi-Source Data Temporal Correlation. *Discov. Appl. Sci.* **2025**, *7*, 872. [CrossRef]
35. Marsetič, A.; Pehani, P. Towards Sub-Pixel Automatic Geometric Corrections of Very-High Resolution Panchromatic Satellite Data of Urban Areas. *Remote Sens.* **2019**, *11*, 1097. [CrossRef]
36. Cevik, I.C.; Atik, M.E.; Duran, Z. Investigation of Optimal Ground Control Point Distribution for Geometric Correction of VHR Remote Sensing Imagery. *J. Indian Soc. Remote Sens.* **2024**, *52*, 359–369. [CrossRef]
37. Briand, T.; Monasse, P. Theory and Practice of Image B-Spline Interpolation. *Image Process. Line* **2018**, *8*, 99–141. [CrossRef]
38. Dharmawan, I.A.; Rahadianto, M.A.E.; Henry, E.; Endyana, C.; Aufaristama, M. Application of High-Resolution Remote-Sensing Data for Land Use Land Cover Mapping of University Campus. *Sci. World J.* **2021**, *2021*, 5519011. [CrossRef] [PubMed]
39. Drisya, J.; Sathish Kumar, D.; Roshni, T. Spatiotemporal Variability of Soil Moisture and Drought Estimation Using a Distributed Hydrological Model. In *Integrating Disaster Science and Management: Global Case Studies in Mitigation and Recovery*; Elsevier: Amsterdam, The Netherlands, 2018; pp. 451–460. [CrossRef]
40. Mizen, A.; Thompson, D.A.; Watkins, A.; Akbari, A.; Garrett, J.K.; Geary, R.; Lovell, R.; Lyons, R.A.; Nieuwenhuijsen, M.; Parker, S.C.; et al. The Use of Enhanced Vegetation Index for Assessing Access to Different Types of Green Space in Epidemiological Studies. *J. Expo. Sci. Environ. Epidemiol.* **2024**, *34*, 753–760. [CrossRef] [PubMed]
41. Cui, B.; Zhao, Q.; Huang, W.; Song, X.; Ye, H.; Zhou, X. A New Integrated Vegetation Index for the Estimation of Winter Wheat Leaf Chlorophyll Content. *Remote Sens.* **2019**, *11*, 974. [CrossRef]
42. Gitelson, A.; Merzlyak, M.N. Quantitative Estimation of Chlorophyll-a Using Reflectance Spectra: Experiments with Autumn Chestnut and Maple Leaves. *J. Photochem. Photobiol. B* **1994**, *22*, 247–252. [CrossRef]
43. Wolf, K.; Jäkel, E.; Ehrlich, A.; Schäfer, M.; Feilhauer, H.; Huth, A.; Wendisch, M. Biases in Estimated Vegetation Indices from Observations under Cloudy Conditions. *Biogeosciences* **2025**, *22*, 7797–7817. [CrossRef]
44. Intergovernmental Panel on Climate Change (IPCC). *Good Practice Guidance for Land Use, Land-Use Change and Forestry*; Institute for Global Environmental Strategies for the IPCC: Kanagawa, Japan, 2003.
45. Nowak, D.J.; Crane, D.E. Carbon Storage and Sequestration by Urban Trees in the USA. *Environ. Pollut.* **2002**, *116*, 381–389. [CrossRef] [PubMed]

46. Sun, Y.; Xie, S.; Zhao, S. Valuing Urban Green Spaces in Mitigating Climate Change: A City-wide Estimate of Aboveground Carbon Stored in Urban Green Spaces of China's Capital. *Glob. Change Biol.* **2019**, *25*, 1717–1732. [CrossRef]
47. Wu, Z.; Jiang, M.; Li, H.; Shen, Y.; Song, J.; Zhong, X.; Ye, Z. Urban Carbon Stock Estimation Based on Deep Learning and UAV Remote Sensing: A Case Study in Southern China. *All Earth* **2023**, *35*, 272–286. [CrossRef]
48. Sharifi, A. Remotely Sensed Vegetation Indices for Crop Nutrition Mapping. *J. Sci. Food Agric.* **2020**, *100*, 5191–5196. [CrossRef] [PubMed]
49. Rana, S.; Gerbino, S.; Carillo, P. Study of Spectral Overlap and Heterogeneity in Agriculture Based on Soft Classification Techniques. *MethodsX* **2025**, *14*, 103114. [CrossRef] [PubMed]
50. Ren, H.; Feng, G. Are Soil-adjusted Vegetation Indices Better than Soil-unadjusted Vegetation Indices for Above-ground Green Biomass Estimation in Arid and Semi-arid Grasslands? *Grass Forage Sci.* **2015**, *70*, 611–619. [CrossRef]
51. Pandit, S.; Tsuyuki, S.; Dube, T. Estimating Above-Ground Biomass in Sub-Tropical Buffer Zone Community Forests, Nepal, Using Sentinel 2 Data. *Remote Sens.* **2018**, *10*, 601. [CrossRef]
52. Hodson, T.O. Root-Mean-Square Error (RMSE) or Mean Absolute Error (MAE): When to Use Them or Not. *Geosci. Model Dev.* **2022**, *15*, 5481–5487. [CrossRef]
53. Belgiu, M.; Drăguţ, L. Random Forest in Remote Sensing: A Review of Applications and Future Directions. *ISPRS J. Photogramm. Remote Sens.* **2016**, *114*, 24–31. [CrossRef]
54. Gu, J.; Congalton, R.G. Assessing the Impact of Mixed Pixel Proportion Training Data on SVM-Based Remote Sensing Classification: A Simulated Study. *Remote Sens.* **2025**, *17*, 1274. [CrossRef]
55. Astola, H.; Häme, T.; Sirro, L.; Molinier, M.; Kilpi, J. Comparison of Sentinel-2 and Landsat 8 Imagery for Forest Variable Prediction in Boreal Region. *Remote Sens. Environ.* **2019**, *223*, 257–273. [CrossRef]
56. Roy, D.P.; Kovalskyy, V.; Zhang, H.K.; Vermote, E.F.; Yan, L.; Kumar, S.S.; Egorov, A. Characterization of Landsat-7 to Landsat-8 Reflective Wavelength and Normalized Difference Vegetation Index Continuity. *Remote Sens. Environ.* **2016**, *185*, 57–70. [CrossRef] [PubMed]
57. Aurellia, N.N.; Putra, T.N.R.; Wakano, Q.S.; Ramadya, A.F.; Desenaldo, R.A.; Dharmawan, I.A. Detection of Tree Cover Dynamic on Belitung Island Using Random Forest Regression. *Media Konserv.* **2025**, *30*, 250. [CrossRef]
58. Putra, T.N.R.; Aufaristama, M.; Ahmed, K.; Arief, M.C.W.; Hanafi, R.; Wijatmoko, B.; Dharmawan, I.A. The Potential Use of a Land Trend Algorithm for Regional Landslide Mapping in Indonesia. *Appl. Sci.* **2026**, *16*, 3090. [CrossRef]
59. Fajariani, W.; Hendra, M.; Susanto, D. Estimation of Above Ground Carbon Sequestration in Trembesi (*Albizia saman*) and Johar (*Senna siamea*) at PT Multi Harapan Utama, East Kalimantan. *J. Trop. Biodivers. Biotechnol.* **2020**, *5*, 115. [CrossRef]
60. Yulistyarini, T.; Hadiah, J.T. Carbon Stock Potential of Indonesian Local Fruit Trees, Some Collections of Purwodadi Botanic Garden. *IOP Conf. Ser. Earth Environ. Sci.* **2022**, *976*, 012057. [CrossRef]
61. Lutz, J.A.; Furniss, T.J.; Johnson, D.J.; Davies, S.J.; Allen, D.; Alonso, A.; Anderson-Teixeira, K.J.; Andrade, A.; Baltzer, J.; Becker, K.M.L.; et al. Global Importance of Large-diameter Trees. *Glob. Ecol. Biogeogr.* **2018**, *27*, 849–864. [CrossRef]
62. Lavista, L.; Prasetyo, L.B.; Hermawan, R. Dynamics Change of the Above Carbon Stocks in Bogor Agricultural University, Darmaga Campus. *Procedia Environ. Sci.* **2016**, *33*, 305–316. [CrossRef]
63. Nandal, A.; Yadav, S.S.; Nath, A.J. Trees Outside Forests as Climate Change Mitigation Champions: Evaluating Their Carbon Sequestration Potential and Monetary Value in Maharshi Dayanand University, Rohtak (Haryana), India. *Environ. Monit. Assess.* **2023**, *195*, 995. [CrossRef] [PubMed]
64. Yumnam, J.Y.; Dey, N. Biomass and Carbon Stock of Trees Growing in Cotton University, Guwahati, Assam, India. *Proc. Natl. Acad. Sci. India Sect. B Biol. Sci.* **2022**, *92*, 853–859. [CrossRef]
65. Wang, Z.; Xu, L.; Shi, Y.; Ma, Q.; Wu, Y.; Lu, Z.; Mao, L.; Pang, E.; Zhang, Q. Impact of Land Use Change on Vegetation Carbon Storage During Rapid Urbanization: A Case Study of Hangzhou, China. *Chin. Geogr. Sci.* **2021**, *31*, 209–222. [CrossRef]
66. Schwaab, J.; Meier, R.; Mussetti, G.; Seneviratne, S.; Bürgi, C.; Davin, E.L. The Role of Urban Trees in Reducing Land Surface Temperatures in European Cities. *Nat. Commun.* **2021**, *12*, 6763. [CrossRef] [PubMed]
67. Wu, J.; Wang, Y.; Qiu, S.; Peng, J. Using the Modified I-Tree Eco Model to Quantify Air Pollution Removal by Urban Vegetation. *Sci. Total Environ.* **2019**, *688*, 673–683. [CrossRef] [PubMed]
68. Žalėnienė, I.; Pereira, P. Higher Education For Sustainability: A Global Perspective. *Geogr. Sustain.* **2021**, *2*, 99–106. [CrossRef]
69. Leal Filho, W.; Shiel, C.; Paço, A.; Mifsud, M.; Ávila, L.V.; Brandli, L.L.; Molthan-Hill, P.; Pace, P.; Azeiteiro, U.M.; Vargas, V.R.; et al. Sustainable Development Goals and Sustainability Teaching at Universities: Falling behind or Getting Ahead of the Pack? *J. Clean. Prod.* **2019**, *232*, 285–294. [CrossRef]